Optics Letters

Fiber-integrated hybrid achromatic microlenses by combined femtosecond laser 3D printing

Liqun Xu,[1,2] Xinyu Gui,[1] Chaowei Wang,[1,4] Xinghao Wang,[1] Yuhang Xue,[1] Yuan Tao,[1] Shengying Fan,[3] Jiawen Li,[1] Jiaru Chu,[1] and Yanlei Hu[1,*]

[1]CAS Key Laboratory of Mechanical Behavior and Design of Materials, Department of Precision Machinery and Precision Instrumentation, University of Science and Technology of China, Hefei 230026, China
[2]Circuit Fabology Microelectronics Equipment Co., Ltd., Hefei 230088, China
[3]Laser Institute, Qilu University of Technology (Shandong Academy of Sciences), Jinan, Shandong 250104, China
[4]chaoweiw@ustc.edu.cn
*huyl@ustc.edu.cn

Received 26 August 2024; revised 25 October 2024; accepted 28 October 2024; posted 29 October 2024; published 26 November 2024

Compact achromats for visible wavelengths are crucial for miniaturized and lightweight full-color endoscopes. Emerging femtosecond laser 3D printing technology offers new possibilities for enhancing the optical performance of miniature imaging lenses on fibers. In this work, we combine refractive and diffractive elements with complementary dispersive properties to create thin, high-performance hybrid achromatic lenses within the visible spectrum, avoiding the use of different optical materials. Using a fiber-integrated hybrid achromatic lens array, clear images are captured across different wavelengths. The fabrication process is carried out using femtosecond laser direct writing (DLW) assisted by femtosecond projection lithography based on a digital micromirror device (DMD). Our work is expected to significantly contribute to the advancement of integrated and miniaturized biomedical imaging devices.

https://doi.org/10.1364/OL.540284

Endoscopes, as the most successful biomedical application of optical fibers, can penetrate deep into the body to obtain clear images of lesions, playing a crucial role in disease diagnosis and treatment [1]. Despite the widespread application of endoscopic technology, improvements are still needed, particularly in developing miniaturized high-resolution endoscopes capable of imaging small and narrow body cavities [2]. However, commercially available endoscopic imaging lenses are restricted in geometry and dimensions due to the limitations of manufacturing [3]. The combination of laser 3D micro-/nano-printing [4] based on two-photon polymerization (TPP) and on-fiber devices [5] can reduce the size of the endoscope to the micron scale [6,7] while providing numerous design freedoms simultaneously, which helps to reduce various aberrations and improve the performance of optical devices [8]. Nevertheless, chromatic aberration remains a major challenge for color imaging in endoscopes, as it prevents the lens from focusing different wavelengths of light on a single point, resulting in blurred color images [9].

It is well known that combining the positive and negative lenses with different refractive indices can effectively reduce chromatic aberration [10]. However, this classical approach requires the use of the two distinct optical materials, which increases the difficulty of positioning and packaging optical elements. Additionally, the large volume of the doublet lens is limited in terms of miniaturization. Diffractive lenses [11] such as metalenses [12] possess the potential to match or exceed the performance of traditional optical lenses while maintaining an ultrathin profile. However, current achromatic diffractive lenses are limited to applications involving infrared wavelengths or low numerical apertures (NAs), due to significant trade-offs among NA, shortest wavelength, and the minimum feature size [13]. To avoid these trade-offs, nanopillars with higher aspect ratios and more complex geometries need to be fabricated, which poses a significant challenge to the mechanical properties of photopolymers. However, diffractive lenses with an Abbe number independent of optical materials have dispersion properties that are the opposite of refractive lenses, so the introduction of diffractive optical elements on refractive lenses can also reduce chromatic aberration and make optical imaging systems lighter [14].

In addition, the improvement of the processing efficiency of laser 3D printing lenses has always been highly concerned. In 2021, Hu *et al.* proposed a DRS-TPP processing technique. This technique first uses a low-power femtosecond laser to accurately define the outer contour of the structure, then uses a high-power femtosecond laser for enhanced scanning to improve the mechanical stability of the structure, and finally uses an ultraviolet (UV) light to quickly expose the unreacted resin inside the structure [15]. This method can effectively shorten the processing time of the lenses, but the UV curing step after development brings additional time consumption. For example, Hu *et al.* used TPP to treat the outer shell of a 400 μm insect compound eye lens in their subsequent work, which only took about 1.5 h, but the developed sample needed to be irradiated under a high-power UV lamp for 12 h [16]. Despite the potential of hybrid

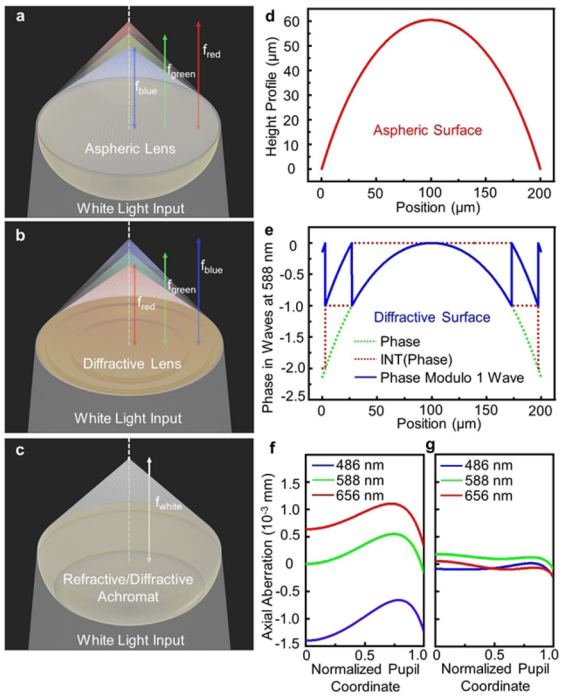

Fig. 1. Design strategy of the hybrid achromatic microlens. Chromatic aberration of (a) refractive lens and (b) diffractive lens. (c) Hybrid achromats utilize the dispersion properties of diffractive elements, which are opposite those of refractive elements to diminish dispersion effects. (d) Radial contour of the designed aspherical base. (e) Radial phase of the designed diffraction layer (dashed green line). The dashed red and solid blue lines represent the integer and decimal parts of the phase, respectively. Axial chromatic aberration of (f) initial aspherical lens and (g) hybrid refractive/diffractive lens.

achromatic lenses to advance to the tip of optical fibers, they still face significant challenges in terms of efficient true 3D processing, limiting their scalability.

In this paper, we combine refractive and diffractive optical elements to form a hybrid refractive/diffractive achromatic lens. By crafting the contours of the aspheric lens and diffraction layer, we successfully achieved a balanced optimization of the on-fiber imaging lens, resolving various aberrations including chromatic aberration for realizing high imaging quality. Considering the fact that the hybrid achromatic lens requires high surface precision but lower internal precision, we employ a digital micromirror device (DMD) femtosecond projection lithography (FPL) technology [17] for rapid internal construction, while the femtosecond laser direct writing (DLW) technology [18] is used for fine scanning of the surface layer with a sawtooth-embossed structure. Finally, using this hybrid femtosecond laser 3D printing strategy, a 2×2 array consisting of four hybrid achromatic lenses (including the frames) is integrated onto the imaging fiber end face, and the function of achromatic imaging is subsequently tested. This work provides a promising perspective for full-color endoscopy.

Within the visible spectrum (400–760 nm), the Abbe number V_r of a refractive lens is always a positive number, meaning that the focal length is shorter for blue light and longer for red light, as shown in Fig. 1(a). Unlike refractive lenses, the dispersion of a diffractive lens is independent of the lens material and only depends on the wavelength band of the light used, and its Abbe number V_d is a negative number, indicating that the focal length is longer for blue light and shorter for red light, as shown in Fig. 1(b). Chromatic aberration can be corrected using two optical elements when the following constraint condition is met: $P_1/V_1 + P_2/V_2 = 0$, with P_i as the focal power of the i-th lens and V_i as the Abbe number. Thus, achromatism can be achieved by combining refractive and diffractive lenses and utilizing their complementary positive and negative dispersions . Moreover, this hybrid achromatic lens requires only a single refractive material [Fig. 1(c)].

In order to achieve comprehensive optimization of the hybrid refractive/diffractive lens, ZEMAX was used to carry out the optical design. First, F-, d-, and C-lines were chosen as the design wavelengths (with the primary wavelength being the d-line at 588 nm). The clear aperture was set to 200 μm, the thickness to 60 μm, and the focal length to 170 μm, with the refractive index of the observing medium as ~1.52. Next, an "even aspheric" surface was chosen to construct the initial structure of the lens. Finally, the surface profile was altered to "Binary2" and further optimized. Figures 1(f) and 1(g) show the axial aberrations of the initial aspheric lens and the hybrid refractive/diffractive lens at different visible wavelengths of 486, 588, and 656 nm, respectively. The aspheric lens exhibits significant chromatic aberration. In contrast, the comprehensively optimized hybrid refractive/diffractive lens, despite having relatively restrained phase modulation depth in the diffraction layer [Fig. 1(e)], demonstrates reduced axial aberrations, indicating its ability to combine excellent achromaticity, precise focusing, and promising imaging quality.

The contour height data of the hybrid refractive/diffractive lens $H_{total}(\rho)$ is calculated as follows:

$$H_{total}(\rho) = H_r(\rho) + H_d(\rho). \quad (1)$$

Here, $H_r(\rho)$ represents the contour height of the aspheric base [Fig. 1(d)], which satisfies the following equation:

$$H_r(\rho) = C\rho^2 / \left[1 + \sqrt{1 - (K+1)C^2\rho^2}\right] + \sum_{i=1}^{8} A_{2i}\rho^{2i}, \quad (2)$$

where C is the curvature, K is the conic constant, ρ is the radial coordinate, and A_{2i} describes the aspheric coefficients. The height contour of the diffraction layer $H_d(\rho)$ can be expressed as follows:

$$H_d(\rho) = \lambda\Phi(\rho)/(n-1) - \lambda\{\mathrm{int}[\Phi(\rho)+1]\}/(n-1), \quad (3)$$

in which $\Phi(\rho) = \sum_i C_{2i}\rho^{2i}/\lambda$ is the phase of the diffraction layer, λ is the wavelength, n is the refractive index of the lens, and C_{2i} represents the phase coefficients.

The hybrid refractive/diffractive lens has a relatively large spatial volume, and using DLW to process the entire structure individually would result in prohibitive time costs, making large-scale production unfeasible. Given that the surface of the hybrid refractive/diffractive lens modulates the light wave, while the internal structure merely serves as a support, a combined femtosecond 3D printing strategy is adopted to enable rapid fabrication. Specifically, FPL is utilized for layer-by-layer patterned exposure of the internal structure, followed by DLW for fine three- dimensional scanning of the surface layer, as shown in Fig. 2(a). The DLW system uses a femtosecond oscillator with a central wavelength of 800 nm (repetition rate: 80 MHz) as the light source, while the FPL system uses a femtosecond amplifier with higher single-pulse energy (repetition rate:

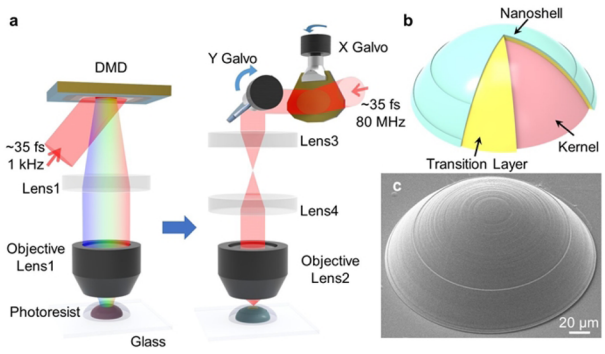

Fig. 2. Fabrication and characterization of the hybrid refractive/diffractive achromatic lens. (a) Manufacturing systems and steps for the hybrid refractive/diffractive lens. (b) Schematic diagram of the three-dimensional structure of the hybrid refractive/diffractive lens. (c) SEM micrograph of the hybrid refractive/diffractive lens obtained by hybrid femtosecond laser 3D printing strategy.

1 kHz) to drive the TPP process. Unlike DLW, which constructs planar structures point-by-point using a dual-axis galvanometer scanner, FPL reconstructs the digitized mask loaded onto the DMD using a 4f system composed of lens1 and objective lens1 (40×, NA = 1.30) to expose the corresponding 2D pattern in a single shot. Figure 2(b) illustrates the structural splitting principle of the hybrid lens. The red part is the core of the lens, and the surface layer is further subdivided into a nanoshell (thickness: 0.4 μm) and a transition layer (thickness: 1.6 μm), which is used to improve the bonding strength between the surface and the interior and to compensate for alignment errors. The photoresist SZ2080 (IESLFORTH, refractive index: ~1.52) mixed with 1 wt. % 4,4-Bis(diethylamino)benzophenone (BIS) with an absorption maximum at 368 nm (Sigma-Aldrich GmbH) was used for all 3D structures in the experiments [19]. After FPL processing, the sample is immediately transferred to the processing platform of DLW. With the assistance of a microscopic imaging system and a three-dimensional electric displacement stage, the center of the lens core gradually aligns with the processing origin. In order to achieve a balance between the service life of the scanning mirror and the scanning speed, the single point exposure time of the DLW process is fixed at 400 μs. A large scan step (400 nm) and a high-power femtosecond laser (22 mW) were selected for rapid scanning of the transition layer. A small scan step (100 nm) and low-power femtosecond laser (15 mW) were chosen for precise definition of the nanoshell, thus further reducing manufacturing time. The entire processing time was about 155.3 min, of which FPL accounted for approximately 5 s (the processing time used by FPL is calculated under the following conditions: layer spacing of 0.5 μm, exposure time of each layer at 40 ms, and laser power of 65 mW). Figure 2(c) shows the scanning electron microscope (SEM) image of the hybrid refractive/diffractive achromatic lens, with clearly visible steps on the diffractive surface.

The achromatic focusing performance of the hybrid refractive/diffractive lens was characterized using a homebuilt test system, as shown in Fig. 3(a). A tunable beam based on a collimated white light-emitting diode (LED) source and different filters is injected onto the fabricated hybrid achromatic lens. An objective lens (20×, NA = 0.45), a focusing lens, and a charge

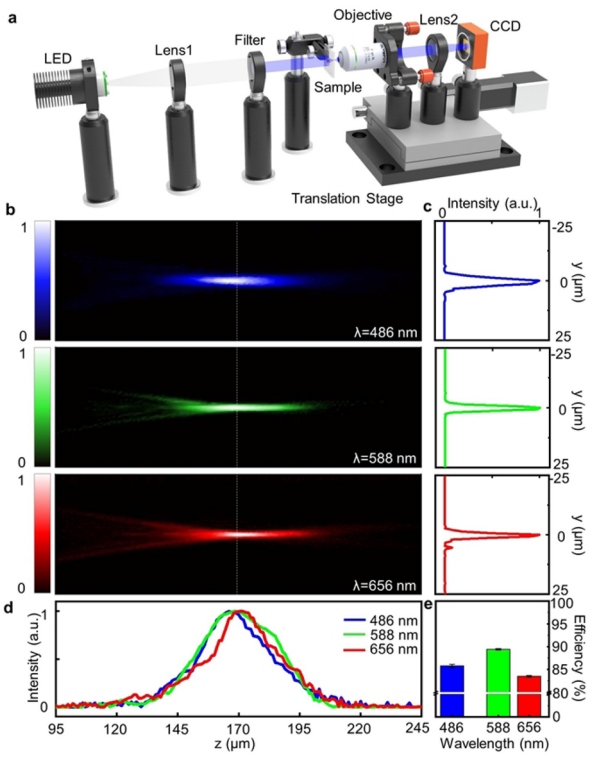

Fig. 3. Measured focusing performance of the refractive/diffractive achromat at visible wavelengths. (a) Experimental optical setup used to characterize the focusing properties of the fabricated hybrid refractive/diffractive achromatic microlens. (b) 2D through focus measurements for the hybrid achromatic lens at 486, 588, and 656 nm. (c) Radial and (d) axial normalized intensity profiles along the symmetry axes of the foci. (e) Focusing efficiencies of the hybrid achromatic lens.

coupled device (CCD) are fixed on a one-dimensional motorized stage, forming a microscopic imaging system capable of capturing transverse beam profiles at different axial positions (with an axial step size of 1 μm with a 150 μm travel range). Figure 3(b) presents the axial profiles of the focal points obtained experimentally at three different wavelengths: 486, 588, and 656 nm, respectively. Additionally, the normalized intensity distributions along the symmetry axes of the foci are shown in Figs. 3(c) and 3(d). The results confirm that the measured axial focal positions are almost the same at different wavelengths, verifying that the printed hybrid refractive/diffractive lens is achromatic with optimized focusing performance. To measure the focusing efficiency of the hybrid refractive/diffractive lens, we assessed the power in the focal spot (the power of transmitted light in a circular area with a radius three times the full width at half maximum) and divided by the incident light power (the power of light incident through a circular area matching the lens radius). The focusing efficiencies of the hybrid achromatic lens at wavelengths of 486, 588, and 656 nm were 85.8, 89.4, and 83.5%, respectively [Fig. 3(e)].

To demonstrate the feasibility of developing the hybrid achromatic lens array with the potential to construct larger area images on fibers, a square array consisting of four hybrid refractive/diffractive lenses was directly printed onto the end face of an imaging fiber. According to the Gaussian imaging law, each lens was manufactured onto a support with a height equal to the focal

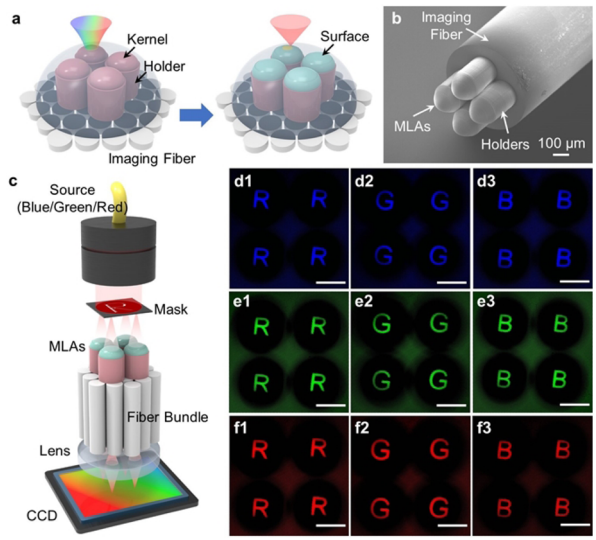

Fig. 4. Manufacturing and imaging of a square array of four hybrid refractive/diffractive achromatic lenses on a fiber bundle. (a) 3D schematic diagram of the processing process. (b) SEM image of the array of four hybrid refractive/diffractive achromatic lenses symmetrically arranged in a square configuration on the tip of the imaging fiber. (c) Schematic diagram of the imaging testing system. Under (d1)–(d3) blue light, (e1)–(e3) green light, and (f1)–(f3) red light, square image arrays of the letters "R," "G," and "B" of the negative masks were obtained. All scale bars: 100 μm.

length in order to image an object at "infinity" on the end face of the imaging fiber. Figure 4(a) illustrates the fabrication process. In the first step, FPL is used to process the 2×2 array structure, which consists of a 2×2 array of pillars with a height of 170 μm and a diameter of 210 μm, and a 2×2 array of lens cores on top of the pillars. In the second step, DLW is used to scan the surfaces of the four lenses individually. The entire process took about 623 min, with FPL accounting for approximately 2 min and DLW accounting for approximately 621 min. In contrast, processing the entire structure using only DLW would require about 3349.7 h, making the hybrid 3D printing strategy over 320 times more efficient. Figure 4(b) shows the SEM test image of the 2×2 array of hybrid refractive/diffractive lenses printed on the end face of the imaging fiber. The results indicate that the fiber-coupled hybrid achromatic lens array obtained using the hybrid 3D printing technology demonstrates an excellent surface quality and a high geometric precision.

The practical value of the fiber-integrated hybrid refractive/diffractive achromatic lens ultimately depends on its achromatic imaging performance. The experimental setup is shown in Fig. 4(c), where different LEDs are used to obtain narrowband red, green, and blue light sources with central wavelengths of 486, 588, and 656 nm, respectively. At the output end of the imaging fiber, a microscope objective lens (10×, NA = 0.30) is used to collect images from the other end of the fiber and input them into a CCD. The image plane diameter of each microlens is about 200 μm, covering approximately 2800 pixels of the imaging fiber. Since the pixel diameter is 4 μm, the image resolution is limited by this specific fiber geometry. Figures 4(d1)–(d3), 4(e1)–(e3), and 4(f1)–(f3) show test results obtained from the fiber lens array under different transmission lights. Blue, green, and red images of quadrilateral arrays with negative masks of the letters "R," "G," and "B" are obtained. The clear imaging effect indicates that the hybrid achromatic endoscope possesses good achromatic performance. Moreover, hybrid femtosecond laser 3D printing technology provides an economically viable route for the mass production of fiber-coupled microlens arrays that can theoretically support a large viewing angle and infinite depth of field.

In summary, this paper proposes a fiber-coupled hybrid refractive/diffractive achromatic lens (array) for visible light, which successfully achieves the correction of chromatic aberration and high imaging performance while avoiding the use of different materials. This method offers a compact configuration without the limitation of numerical aperture. With the high-resolution, high-throughput combined femtosecond 3D printing strategy, this achievement is expected to play a significant role in fields such as life sciences and medicine and contribute to the development of commercially available full-color endoscopes. In the future, our combined femtosecond laser 3D printing should also develop more universal methods to avoid alignment errors, so that this process can be extended to other structures.

Funding. National Natural Science Foundation of Anhui (2408085MF151); Jinan "20 New Universities" Funding Project (202333010); Chinese Academy of Sciences Project for Young Scientists in Basic Research (YSBR-049); National Natural Science Foundation of China (62325507, 52122511, 62105090, 62205236, 52375582, 62475252); National Key Research and Development Program of China (2021YFF0502700).

Acknowledgment. We acknowledge the Experimental Center of Engineering and Material Sciences at USTC for the fabrication and measuring of samples. This work was partly carried out at the USTC Center for Micro and Nanoscale Research and Fabrication.

Disclosures. The authors declare no conflicts of interest.

Data availability. Data underlying the results presented in this paper are not publicly available at this time but may be obtained from the authors upon reasonable request.

REFERENCES

1. B. E. Bouma, M. Villiger, K. Otsuka, *et al.*, Biomed. Opt. Express **8**, 2660 (2017).
2. T. Gissibl, S. Thiele, A. Herkommer, *et al.*, Nat. Photonics **10**, 554 (2016).
3. G. Kostovski, P. R. Stoddart, and A. Mitchell, Adv. Mater. **26**, 3798 (2014).
4. M. He, Z. Zhang, C. Cao, *et al.*, PhotoniX **3**, 25 (2022).
5. Y. Xiong and F. Xu, Adv. Photonics **2**, 064001 (2020).
6. C. Xiong, C. Liao, Z. Li, *et al.*, Front. Mater. **7**, 586496 (2020).
7. L. Xu, C. Wang, X. Qi, *et al.*, Appl. Phys. Lett. **119**, 131101 (2021).
8. B. Li, C. Liao, Z. Cai, *et al.*, Fundam. Res. **4**, 123 (2024).
9. C.-F. Pan, H. Wang, H. Wang, *et al.*, Sci. Adv. **9**, eadj9262 (2023).
10. Z. Y. Hu, T. Jiang, Z. N. Tian, *et al.*, Laser Photonics Rev. **16**, 2100537 (2022).
11. X. Wang, S. Liu, L. Xu, *et al.*, Laser Photonics Rev. **18**, 2300880 (2024).
12. D. Zhang, C.-T. Xu, Q.-M. Chen, *et al.*, PhotoniX **5**, 17 (2024).
13. M. He, X. Shen, X. Liu, *et al.*, Opt. Lett. **48**, 5221 (2023).
14. M. Schmid, F. Sterl, S. Thiele, *et al.*, Opt. Lett. **46**, 2485 (2021).
15. Z.-Y. Hu, H. Ren, H. Xia, *et al.*, J. Lightwave Technol. **39**, 2091 (2021).
16. Z.-Y. Hu, Y.-L. Zhang, C. Pan, *et al.*, Nat. Commun. **13**, 5634 (2022).
17. P. Somers, Z. Liang, J. E. Johnson, *et al.*, Light: Sci. Appl. **10**, 199 (2021).
18. B. Dong, B. Liu, C. Chen, *et al.*, Opt. Lett. **48**, 2508 (2023).
19. A. Ovsianikov, J. Viertl, B. Chichkov, *et al.*, ACS Nano **2**, 2257 (2008).